RSC Advances

PAPER

View Article Online
View Journal | View Issue

Cite this: *RSC Adv.*, 2020, **10**, 21867

Crystal structure, optical spectroscopy and energy transfer properties in $NaZnPO_4:Ce^{3+}$, Tb^{3+} phosphors for UV-based LEDs †

K. Saidi and M. Dammak *

Received 9th May 2020
Accepted 2nd June 2020

DOI: 10.1039/d0ra04163g

rsc.li/rsc-advances

A new series of Ce^{3+}, Tb^{3+} singly doped and Ce^{3+}/Tb^{3+} co-doped $NaZnPO_4$ (NZPO) phosphors have been synthesized *via* a high-temperature solid-state reaction method at 800 °C. The crystal cell structure, luminescence proprieties, energy transfer, and chromaticity coordinates of the as-prepared phosphors were investigated in detail. The photoluminescence spectra of NZPO:Ce^{3+} phosphors exhibited broad emission in the 300–380 nm range, while under UV excitation, the singly doped NZPO:Tb^{3+} phosphor showed emission peaks at ~485–690 nm among which the green emission peak appears at ~543 nm. The Tb^{3+} green emission was significantly enhanced almost 20 times *via* energy transfer from Ce^{3+} to Tb^{3+}. The energy transfer (ET) mechanism from Ce^{3+} to Tb^{3+} in NZPO is identified to be a resonant type *via* the dipole–dipole interaction mechanism with an ET efficiency of 91%. Intense green emission is obtained at very low Tb^{3+} concentrations under 285 nm excitation, making NZPO:Ce^{3+}/Tb^{3+} an efficient UV-excited green phosphor. The $NaZnPO_4:Ce^{3+}/Tb^{3+}$ phosphors are promising UV convertible materials of green light for UV -LEDs applications.

Introduction

Recently, inorganic luminescent materials have attracted great interest by virtue of their wide range of applications such as in white light-emitting diodes, vacuum fluorescent displays, X-ray imaging scintillators, plasma display panels, and field emission displays (FEDs). Luminescent materials have been widely investigated for their many advantages, such as intense brightness, long service life, facile preparation, and being environmental-friendly.[1–4] Rare earth (RE^{3+}), transition metals, and Bi^{3+}-activated phosphors have been extensively investigated due to their unique luminescence performance.[5–9] RE ions can emit fascinating colors thanks to their special 4f shell configuration. Different excitation energies and almost all of the visible light spectrum from violet to red can be obtained by combining different RE ions and varying the ratio of dopants. The Tb^{3+} rare-earth ions are good green-emitting activators due to their dominant green emission peaking around 544 nm which is attributed to $^5D_4$–$^7F_5$ transitions. However, trivalent Tb^{3+} ions have weak absorption in the near-UV range due to 4f–4f strictly forbidden transitions.

On the other hand, the trivalent Ce^{3+} admits broad absorption in the near-UV due to the parity-allowed 4f → 5d transition. It is one of the most excellent sensitizers for WLEDs due to the parity-allowed 4f → 5d transitions. Since the 5d orbital is exposed in the outer electron shell and strongly interacts with its crystalline field, the Ce^{3+}emission wavelength is usually concentrated on the UV and blue light regions.[10,11] Ce^{3+} ions can efficiently absorb near-UV light and yield broad blue emission. Thus, the energy absorbed by Ce^{3+} (sensitizer) is expected to be transferred to Tb^{3+} (activator) in an appropriate host.

Phosphates based phosphors having the general formula $ABPO_4$ (A = monovalent and B = divalent cations) possess excellent physicochemical properties, optical stabilities, better color rendering index (CRI), low phonon energy, good thermal, mechanical and chemical stability. This leads to producing luminescent materials with high the luminescence efficiency for practical applications.[12–14] Among the phosphates-based materials, the sodium zinc *ortho*-phosphate ($NaZnPO_4$) presents excellent coordination flexibility and strong Zn–O–Zn linkages within the lattice. Materials with such properties may improve the PL performance.[15] On the other hand, luminescence of Ce^{3+} and Tb^{3+} ions have gotten actual applications in lightings, detections, and displays.[10,16,17]

Recently, various host materials for Ce/Tb system have been reported for lighting applications including $Sr_2LiScB_4O_{10}:Ce^{3+}/Tb^{3+}$,[17] $K_2CaP_2O_7:Ce^{3+}/Tb^{3+}$,[18] $MgZn_2(PO4)_2:Ce^{3+}/Tb^{3+}$ (ref. 19) and $SrMgSi_2O_6:Ce^{3+}/Tb^{3+}$.[20] Still, there is a demand for novel single-phase green-emitting phosphors with high-efficiency transfers for UV-LEDs applications.

In the previous reports, the properties of $NaZnPO_4$ phosphors doped rare-earth ions have been studied by some

Département de Physique, Faculté des Sciences de Sfax, Laboratoire de Physique Appliquée, Groupe de Physique des Matériaux Luminescents, Université de Sfax, 3018 Sfax, Tunisia. E-mail: madidammak@yahoo.fr

† Electronic supplementary information (ESI) available. See DOI: 10.1039/d0ra04163g

researchers.[14,21,22] However, to enrich the color of the emitted light and to improve the luminescent performance, it is necessary to choose other dopant ions for $NaZnPO_4$ phosphor materials. To the best of our knowledge, the luminescence properties and energy transfer between Ce^{3+} and Tb^{3+} in this host lattice have not been discussed so far. In the present work, we have synthesized single-phase $NaZnPO_4$:(Ce^{3+}, Tb^{3+}) by a solid-state reaction. The crystal structure of the doped materials was discussed. The photoluminescence (PL) properties, the energy transfer mechanism between the sensitizer and activator, and the color chromaticity under UV light have been studied in detail. These results demonstrated the potential applications of NZPO:Ce^{3+}/Tb^{3+} phosphors for solid-state lighting and UV-pumped LEDs.

Experimental section

A series of samples with nominal chemical formulas $NaZnPO_4$ doped $x$$Ce^{3+}$ (x = 0.02, 0.03, 0.04, 0.05, 0.06 and 0.08), $y$$Tb^{3+}$ (y = 0.02, 0.04, 0.06, 0.08, 0.10 and 0.12) and co doped $x$$Ce^{3+}$/$y$$Tb^{3+}$ (abbreviated as NZPO:$x$$Ce^{3+}$/$y$$Tb^{3+}$, where x and y are the molar concentrations), were prepared by a solid-state reaction route at high temperature. The chemical reaction of the $NaZnPO_4$ host compound is given below:

$$Na_2CO_3 + 2ZnO + 2NH_4H_2PO_4 \rightarrow 2NaZnPO_4 + 2NH_3\uparrow + CO_2\uparrow + 3H_2O$$

The reactants are: ZnO [analytical reagent (A.R.)], $NH_4H_2PO_4$ (A.R.), Tb_4O_7 (99.99%), Ce_2O_3 (99.9) and Na_2CO_3 (A.R.). They were weighed stoichiometrically and ground thoroughly in an agate mortar. The mixture was first preheated at 400 °C for 6 h, then reground, and finally fired at 800 °C for 4 h. Subsequently, the products were cooled to room temperature (RT) by switching off the muffle furnace and ground into white power.

Characterization techniques

The X-ray diffraction powder patterns were recorded at room temperature on a Bruker D8 Advance (SeriesII-2009) with Cu Kα radiation on the 10–80° 2θ range with operating at 45 kV and 40 mA. Fourier transforms infrared spectroscopy (FTIR) for the titled compounds were recorded at room temperature on Perkin Elmer Spectrum 1000 FT-IR spectrometer in the 400–1400 cm^{-1} range. The photoluminescence excitation (PLE) and photoluminescence (PL) spectra were recorded on a Jobin Yvon Fluoromax-4 Spectrofluorometer (Horiba, USA) equipped with a 150 W Xe lamp used as an excitation source.

Results and discussion

Structure of products

The NZPO host possesses a monoclinic system and the space group $P2_1/n$.[23] This result can be further confirmed by the Rietveld refinement of the NZPO sample shown in Fig. S1.† The result of Rietveld refinement with χ^2 = 2.24 ensures the accuracy in lattice parameters and atomic site occupations listed in Tables S1 and S2.† The Schematic illustration of the crystal structure of NZPO is presented in Fig. S2.† In this host, the Zn site with the 4e Wyckoff position which creates high stress in the lattice. There exist three kinds of Zn^{2+}cation sites (Zn_{10}, Zn_{14}, and Zn_{19}) and three positions of Na^+ sites: Na (6), Na (7), and Na (18) with a coordination number (CN), CN = 6 for Na (6) and Na (7) and CN = 8 for Na (18). The interatomic distances of P–O, Zn–O, and the Na–O for the NZPO sample are listed in Table S3.†

Fig. 1(a) shows the XRD patterns of NZPO, NZPO:0.05Ce^{3+}, NZPO:0.08Tb^{3+} and NZPO:0.05Ce^{3+}, 0.01Tb^{3+} samples, respectively. Fig. 1(b) depicts part patterns of Fig. 1(a) corresponding to the most pronounced diffraction peak.

Obviously, the main diffraction peaks are observed at 18.91°, 20.18°, 21.84°, 27.73°, 29.91° and 35.64° which are assigned to the (1,1,2), (1,0,3), (0,2,0), (1,1,4), (1,2,3) and (3,0,3) planes respectively. The XRD pattern is matching well and the peaks are perfectly indexed. No additional peaks have been found in the XRD pattern which suggests the single-phase formation of the prepared phosphors. The dopant ions such as Ce^{3+} and Tb^{3+} are supposed to occupy the NZPO lattice to substitute Zn^{2+} ions which creates high stress in the lattice.[24,25] The ionic radii of the doped ions are larger than those of Zn^{2+} (the ionic radii of Tb^{3+} is 0.94 Å, Ce^{3+} is 1.07 Å and Zn^{2+} is 0.74 Å). Thus, it can result in

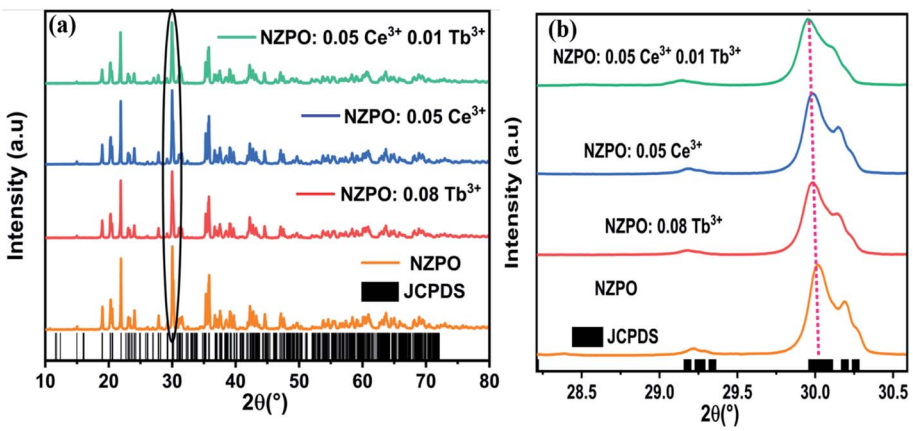

Fig. 1 (a) Powder XRD patterns of NZPO, NZPO:0.05Ce^{3+}, NZPO:0.08Tb^{3+} and NCPO:0.05Ce^{3+}/0.01Tb^{3+} (b) magnified XRD patterns in the region between 28.30 and 30.60°.

Table 1 Lattice Parameters of NZPO, NZPO:0.08Tb^{3+}, NZPO:0.05Ce^{3+} and NZPO:0.05Ce^{3+}/0.01Tb^{3+} samples

Compose	NZPO	NZPO:0.08Tb^{3+}	NZPO:0.05Ce^{3+}	NZPO:0.05Ce^{3+}/0.01Tb^{3+}
a (Å)	8.668	8.670	8.667	8.672
b (Å)	8.131	8.133	8.133	8.135
c (Å)	15.2591	15.262	15.263	15.255
β (°)	89.8007	89.800	89.798	89.7975
V (Å^3)	1075.548	1076.227	1076.195	1076.316

charge imbalance and form charge defects in host lattice when the trivalent rare-earth ions replace the divalent alkaline earth ions. However, the substitution of Ce^{3+} and Tb^{3+} ions could bring the positive charges in the lattices inducing a mismatch of charge on the cation sites that could be balanced by the negative charges, like cation vacancy (V_{Zn}), or interstitial oxygen (O_i). Therefore, the lattice gets enlarged and for which all the peaks in the XRD pattern shifted slightly in the lower angle side compared to the standard JCPDS card no. 79-0217 pattern of the host lattice because of the radius difference,[26,27] as depicted in Fig. 1(b). Rietveld plots of NZPO:0.05Ce^{3+}, NZPO:0.08Tb^{3+} and NZPO:0.05Ce^{3+}/0.01Tb^{3+} are presented in Fig. S3, S4 and S5† respectively. The lattice parameters and the corresponding unit cell volumes of the prepared phosphors were calculated from the diffraction data using Rietveld refinement and listed in Table 1.

FTIR analysis

In order to confirm the phase purity, the functional group analyses were performed by Fourier Transform Infrared (FTIR) spectroscopic method. FTIR spectra of undoped, Tb^{3+}, Ce^{3+} doped and Ce^{3+}/Tb^{3+} codoped $NaZnPO_4$ phosphors are shown in Fig. 2. The observed bands in the 900–1100 cm^{-1} range are assigned to the symmetric and antisymmetric stretching frequencies (PO_4^{3-}). Similarly, the bands located in the 500–630 cm^{-1} range correspond to the asymmetric deformation modes. The absorption band at 472 cm^{-1} is due to symmetric deformation modes of phosphate groups, this band confirms the apatite structure of the phosphate and then the existence of PO_4 tetrahedra in their structures.[22,28] No additional peaks were observed in FTIR spectra which confirm the phase purity of the phosphors. Therefore, the FTIR analysis also supports the XRD results that the synthesized compounds possessed a monoclinic structure.

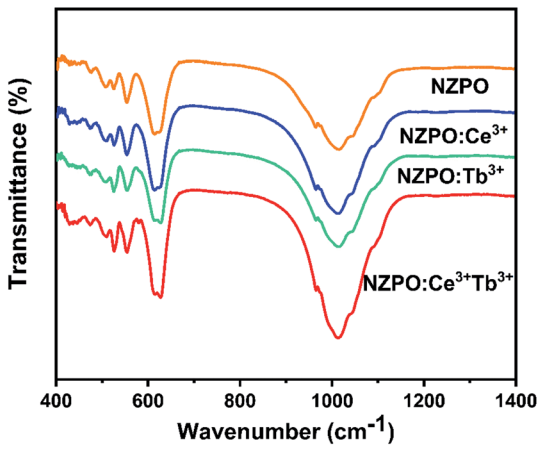

Fig. 2 FTIR transmission spectra of NZPO, NZPO:Ce^{3+}, NZPO:Tb^{3+} and NZPO:Ce^{3+}/Tb^{3+}.

Luminescence properties of Ce^{3+} ions in NZPO phosphors

Fig. 3 exhibits the PLE spectra of $NaZnPO_4$:0.05Ce^{3+} monitored at 319 nm and 341 nm emission wavelengths and the PL spectrum of $NaZnPO_4$:0.05Ce^{3+} under 285 nm excitation.

The PLE spectra NZPO:0.05Ce^{3+} display one band in the 200–300 nm range ($\lambda_{max} \approx 285$ nm), which can be attributed to the transitions from the ground state to the different crystal field splitting levels of the 5d state of the Ce^{3+} ions. The absence of electrons in the 5s and 5p shells makes them in the inner 5d orbital unshielded and exposed to the environment ions. The 5d orbital is the excited energy level for electrons promoted from 4f orbital ground state under UV excitation. It can be seen that the emission spectrum consists of a double band with maximum peaks at approximately 319 nm (31 347.96 cm^{-1}) and 341 nm (29 325.51 cm^{-1}) depicted in the inset with a difference of approximately 1936 cm^{-1} under near-ultraviolet excitation (285 nm).[17,29] This result is in accordance with the theoretical value of $\approx$ 2000 cm^{-1}. The double band emission is observed which verifies one specific lattice site due to the transitions from the relax lowest 5d excited state to the $^2F_{5/2}$ and $^2F_{7/2}$ spin–orbit split 4f ground states (5d $\rightarrow$ $^2F_{5/2}$ and 5d $\rightarrow$ $^2F_{7/2}$). It's worth noting that the similarity of Zn (1), Zn (2), and Zn (3) sites can lead to the one-site luminescent behavior for Ce^{3+}.

Fig. 4(a) and (b) present the concentration-dependent PL spectra of NZPO:Ce^{3+} phosphors upon 285 nm UV excitation, and the concentration dependence of the emitting intensities of

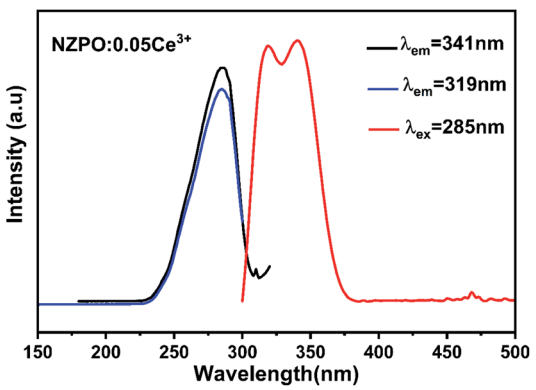

Fig. 3 PLE and PL spectra of NZPO:0.05Ce^{3+}.

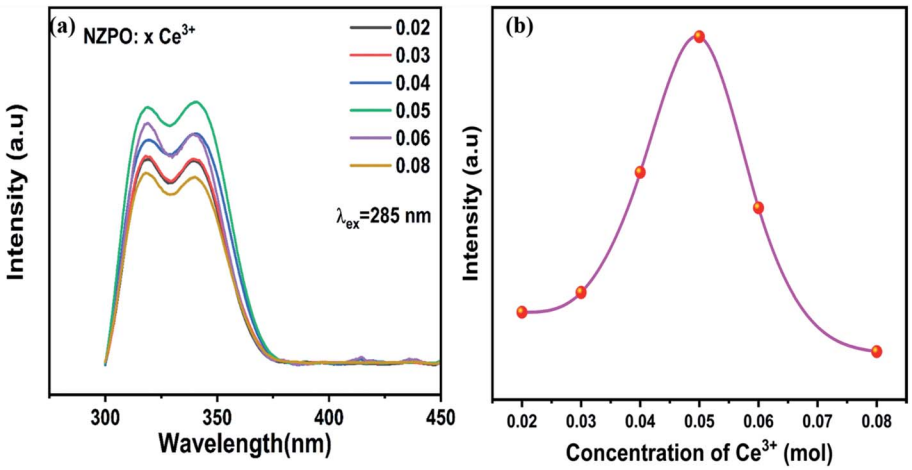

Fig. 4 (a) Concentration-dependent PL spectra of NZPO:xCe^{3+} (x = 0.02, 0.03, 0.04, 0.05, 0.06 and 0.08). (b) Variation of the emission intensity with Ce^{3+}(x) concentration.

NZPO:Ce^{3+} with various Ce^{3+} concentrations, respectively. The emission intensities increase with Ce^{3+} concentration increasing up to 0.05; beyond that, it decreased to the lowest because of the concentration quenching effect. When the x value reaches 0.05, the maximum emission intensity occurs and it was kept as a constant value to prepare Ce^{3+}/Tb^{3+} co-doped NZPO phosphors.

The non-radiative energy transfer mechanism was responsible for the concentration quenching of NZPO:x Ce $^{3+}$ phosphors. The critical distance R_C between Ce^{3+} ions can be estimated using the equation given by Blasse:[30,31]

$$R_c \approx 2\left[\frac{3V}{4\pi x_c Z}\right]^{1/3} \quad (1)$$

where R_c is the critical distance, V is the volume of the unit cell, x_c refers to the critical doping concentration, and Z is the number of formula units per unit cell. For the NZPO host, $Z = 4$, and x_c value is 0.05 for Ce^{3+}. Therefore, the critical distance (R_c) was calculated to be about 21.74 Å. This value excludes the exchange interaction because it is predominant only for about 5 Å.

The concentration quenching mechanism of the Ce^{3+} in the phosphor is dominated by the multipole–multipole interaction. Based on the report of Van Uitert,[32] the relation between emission intensity (I) and doping concentration of Ce^{3+} ions (x) can be expressed as:

$$I/x = k(1 + \beta(x)^{\theta/3})^{-1} \quad (2)$$

where x is the activator concentration, I/x is the emission intensity per activator concentration, k and β are constants for a given host in the same excitation condition, θ = 6, 8 and 10 represent the dipole–dipole(D–D), dipole–quadrupole (D–Q), and quadrupole–quadrupole (Q–Q) interactions, respectively. Assuming that $\beta(x)^{\theta/3} \gg 1$, the above eqn (2) can be written as:[33,34]

$$\mathrm{Log}(I/x) = K' - (\theta/3)\mathrm{Log}(x) \text{ and } K' = \log k - \log \beta \quad (3)$$

Fig. 5 illustrates the relationship between log(I/x) and log(x) and the corresponding straight line with slope referring – θ/3. Herein, the calculated value of θ/3 is 1.4066, and θ can be calculated as 4.2198, which is close to 6. The result indicates that the concentration quenching mechanism of the Ce^{3+} emission in NZPO:Ce^{3+} host is dominated by the dipole–dipole (D–D) interaction.

Luminescence NZPO:Tb^{3+} phosphors

The excitation and emission spectra of Tb^{3+} activated NZPO powders are displayed in Fig. 6. The excitation spectrum of the NZPO:0.08Tb^{3+} monitored at 543 nm presents several bands between 290 and 490 nm, which can be attributed to f–f transitions within the 4f^8 configuration of Tb^{3+}. These bands are attributed to the $^7F_6 \rightarrow {}^5H_6$ (303 nm), $^7F_6 \rightarrow {}^5H_7$ (318 nm), $^7F_6 \rightarrow {}^5L_6$ (341 nm), $^7F_6 \rightarrow {}^5L_9$ (350 nm), and $^7F_6 \rightarrow {}^5G_6$ (375 nm) transitions.[27,35] In Addition, the position of the peaks has not been changed for the 4f electrons of Tb^{3+} ions since they are shielded by 5s^2 5p^6 shells. The emission spectrum is recorded in

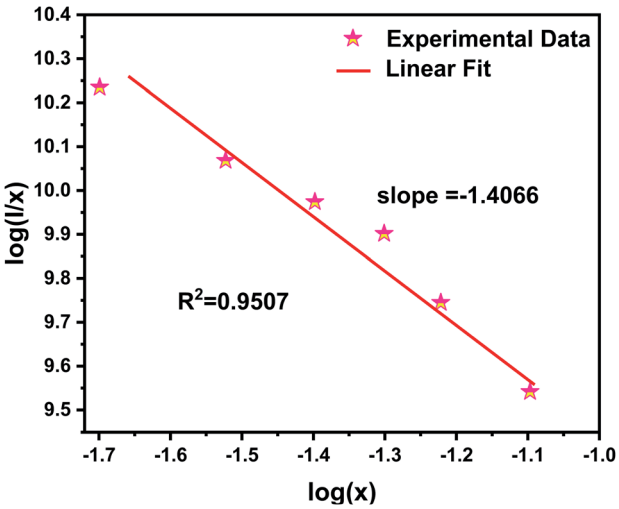

Fig. 5 Linear fitting of log(x) *versus* log(I/x) of NZPO:xCe^{3+} (x = 0.02, 0.03, 0.04, 0.05, 0.06 and 0.08) phosphors.

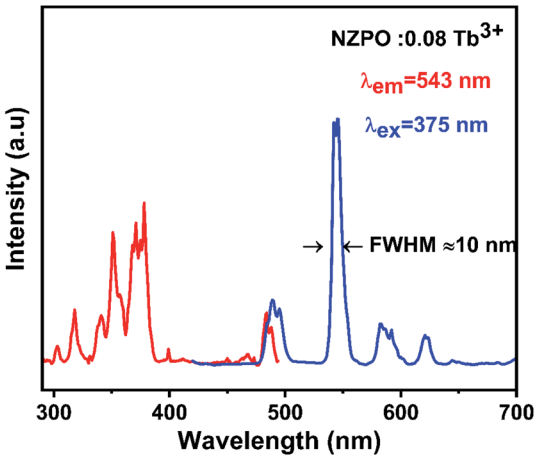

Fig. 6 PL excitation and emission spectra of NZPO:0.08Tb^{3+} monitored at 543 nm and excited at 375 nm.

the range of 400–700 nm by exciting with a UV light at 375 nm. The phosphor shows the emission peaks at 490 nm, 543 nm, 582 nm, and 620 nm, which are assigned to $^5D_4 \rightarrow {}^7F_6$, $^5D_4 \rightarrow {}^7F_5$, $^5D_4 \rightarrow {}^7F_4$ and $^5D_4 \rightarrow {}^7F_3$ transitions, respectively.[35,36] NZPO:0.08 Tb^{3+} can produce a green emission due to the maximum peak at 543 nm corresponding to the $^5D_4 \rightarrow {}^7F_5$ magnetic dipole transition. This green emission peak at 543 nm has an extremely narrow full-width at half-maximum (FWHM) of only about 10 nm, which is narrower than the previously reported green luminescence materials used for display, involving $Ca_2YZr_2(AlO_4)_3$:Tb^{3+} (>13.5 nm), SiO_2:Tb^{3+} (>20 nm), and in the same order then that reported for $LaPO_4$ codoped Ce^{3+}/Tb^{3+} (>7.8 nm).[37–39]

The PL emission intensity of the Lanthanides (Ln^{3+}) doped phosphors is strongly dependent on the activator's concentration. To figure out the optimal doping concentration of Tb^{3+} ions in NZPO host material, a series of Tb^{3+} doped NZPO phosphors were prepared and their luminescent properties were also studied.

Fig. 7 shows the PL spectra of the NZPO:x Tb^{3+} (x = 0.02, 0.04, 0.06, 0.08, 0.10 and 0.12) phosphors as a function of Tb^{3+} ion concentration under 375 nm excitation. The PL emission intensity of the NZPO:Tb^{3+} phosphors first exhibited an increasing tendency with the increase of Tb^{3+} doping concentration and reached a maximum at 0.08Tb^{3+}. This phenomenon is a result of the concentration quenching of the Tb^{3+} ions. It is accepted that the non-radiative energy transfer among Tb^{3+} ions mainly results in the concentration quenching. In order to analyze the energy transfer mechanism between Tb^{3+} in NZPO, the critical distance is needed to be determined eqn (1).

The critical transfer distance R_{Tb-Tb} for energy transfer from Tb^{3+} to Tb^{3+} ions in NZPO phosphors was calculated to be ~18 586 Å. The exchange interaction is not possible between the Tb^{3+} ions because the R_c value is greater than 5 Å. The larger value of R_c indicates that multipolar interaction was responsible for the concentration quenching.

The interaction type between different Tb^{3+} ions can be obtained by the eqn (2) and (3).

Fig. 8 shows the relationship between log(I/x) and log(x) of NZPO:Tb^{3+} phosphor. The slope value of −1.2754 was determined from the linear curve of log(I/x) *versus* log(x). Hence, the θ value was determined to be 3.8262, which is quite close to the theoretical value of 6 corresponding to the D–D interaction. It can be concluded that the D–D interaction is the main mechanism for the concentration quenching.

Luminescence and energy transfer in NZPO:Ce^{3+}/Tb^{3+} phosphors

Fig. 9(a) depicts the PL and PLE spectra of singly Ce^{3+} and Tb^{3+} doped in $NaZnPO_4$ respectively. The overlap between the PL and PLE spectra induces an important energy transfer between the

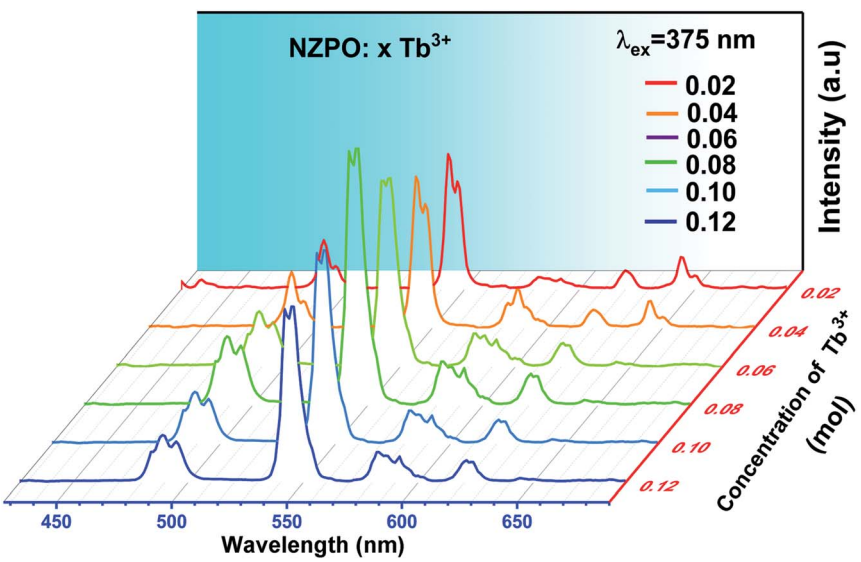

Fig. 7 Emission spectra of NZPO:$x$$Tb^{3+}$ (x = 0.02, 0.04, 0.06, 0.08, 0.10 and 0.12) excited at 375 nm.

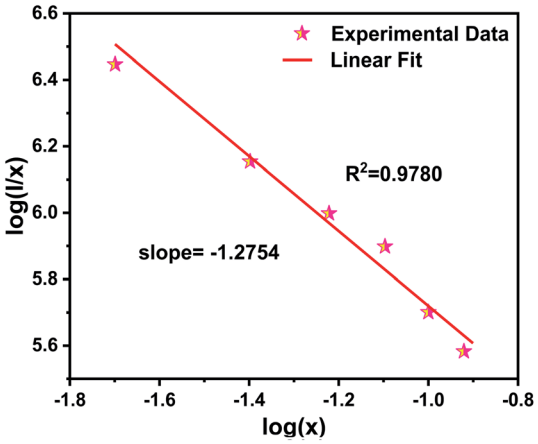

Fig. 8 Linear fitting of log(*I*/*x*) *versus* log(*x*) of ($^5D_4 \rightarrow {}^7F_5$) Tb^{3+} emissions.

Ce^{3+} and Tb^{3+} ions. Generally, Ce^{3+} ions can be introduced as sensitizers to the Tb^{3+} ions to increase the Tb^{3+} emissions.

Fig. 9(b) presents the excitation spectrum of NZPO:0.05 Ce^{3+}/0.08Tb^{3+} supervised at 543 nm (Tb^{3+} emission). This spectrum is similar to that supervised at 319–341 nm (Ce^{3+} emission) except for the difference in the relative intensity. The excitation spectrum shows broad band of Ce^{3+} ion which is attributed to the 4f–5d transition. The presence of the Ce^{3+} transition in the excitation spectra monitored within the Tb^{3+} emissions demonstrates the presence of an energy transfer between the Ce^{3+} and Tb^{3+} ions.[19] In order to further investigate this energy

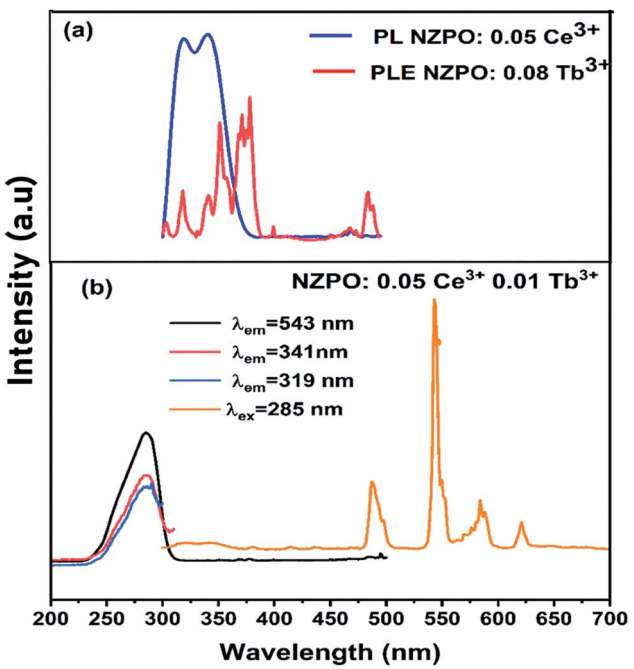

Fig. 9 (a) Spectral overlap between the emission spectrum of NZPO:0.05Ce^{3+} and the excitation spectrum of NZPO:0.02Tb^{3+}. (b) Excitation and emission spectra of NZPO:0.05Ce^{3+}/0.01Tb^{3+} phosphors.

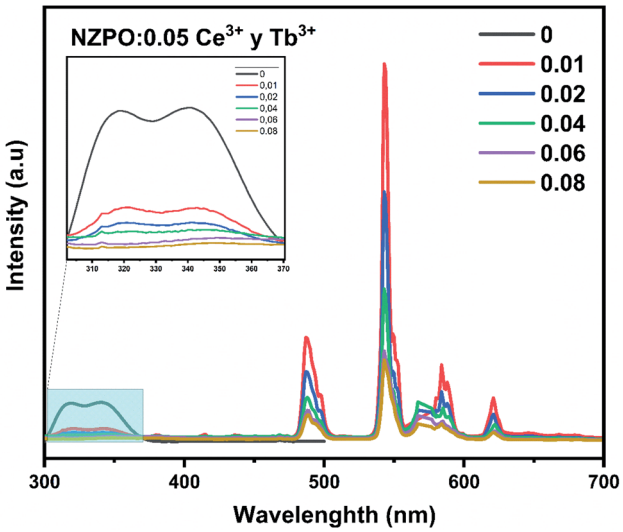

Fig. 10 PL spectra of NZPO:0.05Ce^{3+}/$y$$Tb^{3+}$ (y = 0.00, 0.01, 0.02, 0.04, 0.06 and 0.08) excited at 285 nm.

transfer process, we have investigated the PL spectra of the NZPO:Ce^{3+}/Tb^{3+} co-doped phosphor under 285 nm excitation. The PL spectrum exhibited both, the emission transitions of Ce^{3+} (5d $\rightarrow$ 4f) and those of Tb^{3+} ions ($^5D_4 \rightarrow {}^7F_{3,4,5,6}$). The doping concentration of Ce^{3+} is fixed at the optimal value 0.05, and a series of NZPO:0.05Ce^{3+}, y Tb^{3+} (y = 0, 0.01, 0.02, 0.04, 0.06, 0.08) samples were prepared.

Fig. 10 displays the emission spectra of NZPO:0.05Ce^{3+}/$y$$Tb^{3+}$ (y = 0, 0.01, 0.02, 0.04, 0.06, 0.08) phosphors under 285 nm excitation. The highest intensity green emission of Tb^{3+} (543 nm) was realized for NZPO:0.05Ce^{3+}/0.01Tb^{3+}. We noticed a gradually decreases of the Ce^{3+} PL intensity with Tb^{3+} concentration increasing, as can be clearly seen in Fig. 11. These results confirmed that an effective energy transfer occurred between the Ce^{3+} and the Tb^{3+} ions.

This energy transfer between Ce^{3+} and Tb^{3+} ions can more investigated according to the Dexter model.[40,41]

$$P_{SA} = \frac{2\pi}{h}\left|\langle A, S^*|H_{SA}|A^*, S\rangle\right|^2 \int g_S(E)g_A(E)\mathrm{d}E \qquad (4)$$

where P_{SA} is the energy transfer rate and H_{AS} is the interaction Hamiltonian. The matrix element indicates the interaction between the initial state $|A,S^*\rangle$, and the final state $\langle A^*,S|$. $\int g_S(E)g_A(E)\mathrm{d}E$ integral represents the spectral overlap between the emission spectrum of the sensitizers and the excitation spectrum of activators.

From the apparent overlap between the Tb^{3+} PLE and Ce^{3+} PL spectra and the Dexter eqn (4), it can be concluded that resonance type energy transfer may occur from Ce^{3+} to Tb^{3+} in the NZPO host.

Moreover, the comparison of PL spectra of NZPO:Tb^{3+} and NZPO:Ce^{3+}/Tb^{3+} show that the intensity of green Tb^{3+} emission is higher in the co-doped than that in the doped sample which confirms that Ce^{3+} is an efficient sensitizer ion for Tb^{3+} green emission, as shown in Fig. 12. The overall integrated emission intensity is enhanced of about 20 times in the co-doped sample

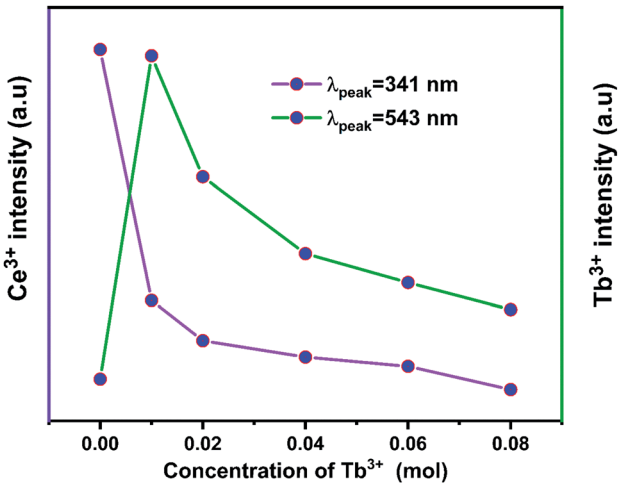

Fig. 11 Dependence of (5d → 4f) Ce^{3+} and ($^5D_4 \rightarrow {}^7F_5$) Tb^{3+} emissions as a function of Tb^{3+} concentration.

(NZPO:0.05Ce^{3+}/0.01Tb^{3+}) when compared to the doped sample (NZPO:0.08 Tb^{3+}).

$Ce^{3+} \rightarrow Tb^{3+}$ energy transfer

The ET efficiency (η_T) of $Ce^{3+} \rightarrow Tb^{3+}$ in NZPO phosphors can be calculated by using the following equation:[37,42]

$$\eta_T = 1 - \frac{I_D}{I_{D0}} \quad (5)$$

where, I_{D0} and I_D are the Ce^{3+} luminescence intensity in both the absence and the presence of Tb^{3+}, respectively.

Fig. 13 illustrated the energy transfers efficiencies in NZPO:0.05Ce^{3+}/xTb^{3+} ($y = 0.01$, 0.02, 0.04, 0.06 and 0.08). It was seen that the energy transfer efficiencies values increase with Tb^{3+} increasing. A maximum $Ce^{3+} \rightarrow Tb^{3+}$ energy transfer efficiency of 91% was obtained for NZPO:0.05Ce^{3+}/0.08Tb^{3+} sample which is found to be higher than that of the similar reported orthophosphate phosphors, such as $NaBaPO_4$:0.04Ce^{3+}/

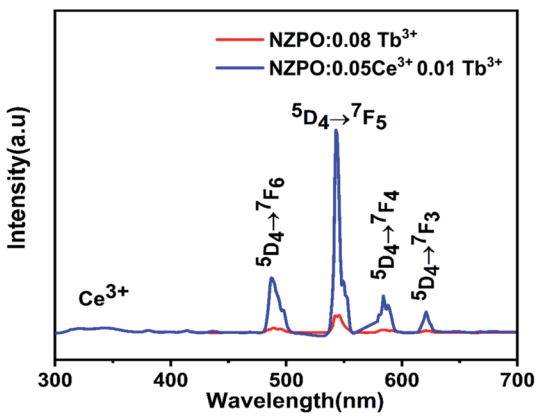

Fig. 12 Comparison of Tb^{3+} emissions of doped NZPO:0.08Tb^{3+} and cooped NZPO:0.05Ce^{3+}/0.01Tb^{3+} phosphors.

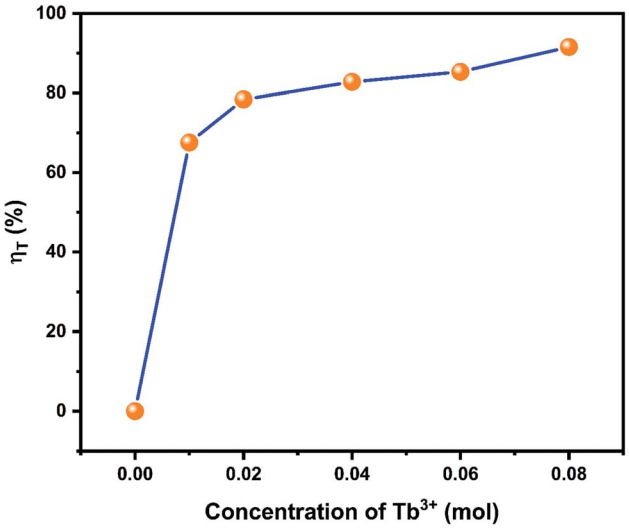

Fig. 13 Dependence of the energy transfer efficiency (η_T) on the Tb^{3+} concentration.

0.15Tb^{3+} (78.8%),[43] $NaCaPO_4$ 0.02 Ce^{3+}/0.12Tb^{3+} (80%),[44] $Ba_3Y(PO_4)_3$:0.05Ce^{3+}/0.45 Tb^{3+} (69.9%).[45]

Generally, two factors can be responsible for the resonant energy transfer mechanism: the exchange interaction and the multipolar interaction.

For the NZPO host, the critical concentration of the dopant (x_c) and the critical separation between the activator and sensitizer (R_c) is calculated to be 0.06 and 20.46 Å respectively (eqn (1)). R_c value is in the same order as that reported for $SrMgSi_2O_6$ Ce^{3+}/Tb^{3+} phosphors (19.52 Å).[20] The R_c calculated value indicates the little possibility of exchange interaction since the exchange interaction is only for about 5–10 Å. Therefore, we can infer the energy transfer mechanism from Ce^{3+} to Tb^{3+} ions are likely to be electric multipolar interactions.[20,46]

According to the Dexter energy transfer and Readfield's approximation, the energy transfer formula for multipolar interactions can be written as:[47,48]

$$\frac{I_{D0}}{I_D} \approx C_{Tb}^{n/3} \quad (6)$$

where C is the concentrations of Tb^{3+} and I_{D0} and I_D are the luminescence intensities of the sensitizer Ce^{3+} in the absence and presence of the activator Tb^{3+},

The values for $n = 6$, 8, 10 are attributed to dipole–dipole, dipole-quadrupole, and quadrupole–quadrupole interactions, respectively.

The relationship curves between I_{D0}/I_D and $C^{n/3}$ are shown in Fig. 14, and the energy transfer model can be judged by comparing the R factors during the linear fitting. It can be inferred that the dipole–dipole interaction is the main energy transfer model between Ce^{3+} and Tb^{3+} ions in the NZPO host which is consistent with the bibliographic results.[20,31,49,50]

Schematic diagram of energy transfer

The schematic diagram of the energy levels of Ce^{3+} and Tb^{3+} with the possible optical transition involved in the energy

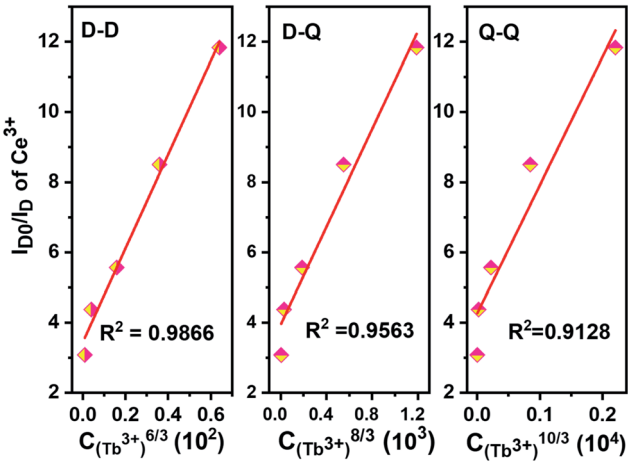

Fig. 14 Dependence of I_{D0}/I_D of Ce^{3+} in NZPO:0.05Ce^{3+}/yTb^{3+} (y = 0.01, 0.02, 0.04, 0.06, 0.08) phosphors.

transfer processes is presented in Fig. S6.† For the NZPO:Ce^{3+}/Tb^{3+} phosphor, the electrons in excited states promote to the excited state of the Tb^{3+} 5d level (energy transfer process), which is attributed to the large overlap between the 4f → 4f transition of Tb^{3+} and the 5d–4f transition of Ce^{3+}. The electrons in the Tb^{3+} 5d level relax to the $^5D_4$ and $^5D_3$ levels, and then the electrons return to ^7F_J (J = 0–6) levels with multiple peaks. However, in this host there are only four peaks that are assigned to $^5D_4 \rightarrow {}^7F_J$ (J = 3, 4, 5, 6), and the other peaks do not appear. This result can be explained by the cross-relaxation with non-radiative transitions from $^5D_3$ to $^5D_4$ states. Finally, the exciting Tb^{3+} ions return to their ground state with subsequent emission of green luminescence.

Commission internationale de l'eclairage (CIE) 1931 diagram

In general, color can be expressed by means of color coordinates and the CIE 1931, which is a two-dimensional graphical representation of any color perceptible by the human eye on an x–y plot. According to the PL spectrum, under 285 nm excitation, Commission International de Eclarite (CIE) chromaticity coordinates of the samples are presented in Fig. 15 and summarized in Table S4.†

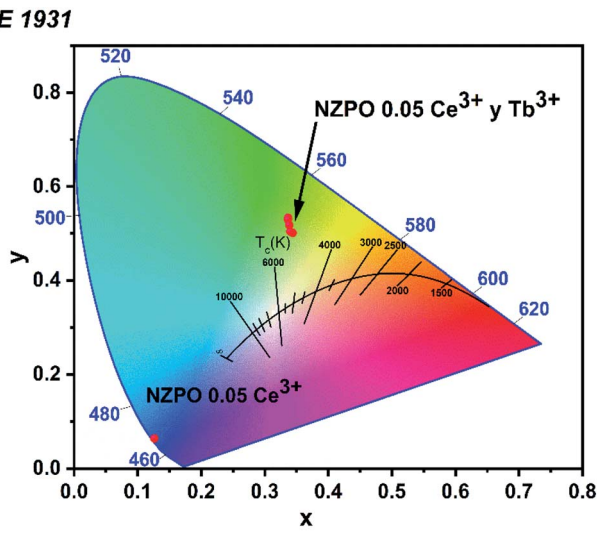

Fig. 15 CIE 1931 color coordinates corresponding to the NZPO:0.05Ce^{3+}/yTb^{3+} (y = 0.00, 0.01, 0.02, 0.04, 0.06 and 0.08) phosphors.

We noticed that the singly Ce^{3+} doped NZPO sample shows dark blue emission under UV excitation. However, 0.05 Ce^{3+} /0.01Tb^{3+} co-doped NZPO sample shows green emission. The CIE chromaticity coordinate of NZPO:0.05Ce^{3+}/0.01Tb^{3+} phosphor is determined to be (0.3149, 0.5652) which is closer to the commercial phosphor $MgAl_{11}O_{19}$:0.67Ce^{3+}/0.33Tb^{3+} (0.330, 0.595). It is found that NZPO:0.05Ce^{3+}/0.01Tb^{3+} shows intense green light suggesting that it can be used as a potential green-emitting candidate for the lighting field.

Conclusions

In summary, a new series of Ce^{3+}, Tb^{3+} singly doped and Ce^{3+}/Tb^{3+} co-doped $NaZnPO_4$ (NZPO) phosphors were successfully prepared *via* the conventional high-temperature solid-state reaction. XRD results and Rietveld refinement analysis show that NZPO:Ce^{3+}, Tb^{3+} crystallized in a monoclinic structure with $P2_1/n$ (14) space group. The photoluminescence spectra of NZPO:Ce^{3+} phosphors exhibited broad emission in the 300–380 nm range with a peak maximum at 341 nm. The photoluminescence emission spectrum of Tb^{3+} singly doped NZPO shows several sharp peaks at 488, 543, 585, and 622 nm related to 4f–4f transitions. Additionally, the dominant green emission band around 543 nm has a full width at half-maximum (FWHM) only about 10 nm. The ET from Ce^{3+} to Tb^{3+} in the NZPO host was studied in detail. The Tb^{3+} green emission was significantly enhanced almost 20 times *via* energy transfer from Ce^{3+} to Tb^{3+}. The ET mechanisms of Ce^{3+} to Tb^{3+} has been determined to be a resonant type by electric dipole–dipole interaction, and the energy transfer efficiency reached a maximum of 91% for NZPO:0.05 Ce^{3+}/0.08Tb^{3+}. This phosphor can be efficiently excited *via* 285 nm excitation to emit intense green light. These resultants demonstrate that the NZPO:Ce^{3+}/Tb^{3+} phosphors are very promising as green-emitting phosphors for lighting applications.

Conflicts of interest

There are no conflicts to declare.

References

1 C. C. Lin and R.-S. Liu, *J. Phys. Chem. Lett.*, 2011, **2**, 1268–1277.
2 X. Huang, *Nature Photon*, 2014, **8**, 748–749.
3 E. M. Chan, *Chem. Soc. Rev.*, 2015, **44**, 1653–1679.
4 G. Li, Y. Tian, Y. Zhao and J. Lin, *Chem. Soc. Rev.*, 2015, **44**, 8688–8713.
5 G. R. Dillip and B. Deva Prasad Raju, *J. Alloys Compd.*, 2012, **540**, 67–74.
6 L. Zhao, Y. Liu, C. Zhai, F. Liao and Y. Gao, *J. Alloys Compd.*, 2017, **694**, 721–725.

7 G. S. Ningombam, N. S. Khundrakpam, D. S. Thiyam, R. S. Ningthoujam and N. R. Singh, *New J. Chem.*, 2020, **44**, 4217–4228.
8 M. Back, J. Ueda, J. Xu, K. Asami, L. Amidani, E. Trave and S. Tanabe, *J. Phys. Chem. C*, 2019, **123**, 14677–14688.
9 M. Back, J. Ueda, M. G. Brik, T. Lesniewski, M. Grinberg and S. Tanabe, *ACS Appl. Mater. Interfaces*, 2018, **10**, 41512–41524.
10 B. Zhang, S. Ying, S. Wang, L. Han, J. Zhang and B. Chen, *Inorg. Chem.*, 2019, **58**, 4500–4507.
11 J. Zhou, Q. Liu and Z. Xia, *J. Mater. Chem. C*, 2018, **6**, 4371–4383.
12 C. C. Lin, Z. R. Xiao, G.-Y. Guo, T.-S. Chan and R.-S. Liu, *J. Am. Chem. Soc.*, 2010, **132**, 3020–3028.
13 Q. Bai, P. Li, Z. Wang, S. Xu, T. Li and Z. Yang, *RSC Adv.*, 2017, **7**, 22301–22310.
14 L. Mukhopadhyay and V. K. Rai, *New J. Chem.*, 2017, **41**, 7650–7661.
15 H. Pan, X. Li, J. Zhang, L. Guan, H. Su and F. Teng, *Mater. Lett.*, 2015, **155**, 106–108.
16 X. Zhang, Y. Huang and M. Gong, *Chem. Eng. J.*, 2017, **307**, 291–299.
17 H. Chen and Y. Wang, *Inorg. Chem.*, 2019, **58**, 7440–7452.
18 Y. Ding, L. Wang, M. Xu, D. Jia and R. Zhou, *J. Am. Ceram. Soc.*, 2017, **100**, 185–192.
19 M. Xu, L. Wang, D. Jia and H. Zhao, *Phys. Chem. Chem. Phys.*, 2015, **17**, 28802–28808.
20 X. Fu, L. Fang, S. Niu and H. Zhang, *J. Lumin.*, 2013, **142**, 163–166.
21 L. Mukhopadhyay and V. K. Rai, *AIP Conf. Proc.*, 2018, **1953**(1), 060021.
22 L. Mukhopadhyay and V. K. Rai, *New J. Chem.*, 2018, **42**, 13122–13134.
23 L. Elammari, J. Durand, L. Cot and B. Elouadi, *Z. Kristallogr. Cryst. Mater*, 1987, **180**, 131–140.
24 G. Dong, X. Li, H. Pan, H. Ma, S. Zhao, L. Guana, P. Duan, N. Fu, C. Liu and X. Lia, *J. Lumin.*, 2019, **206**, 260–266.
25 X. W. Wang, J. G. Chen, Y. W. Tian, X. E. Wang, B. H. Zhang and X. H. Chang, *Solid State Ionics*, 2016, **296**, 85–89.
26 B. Wang, R. Mi, Y. Liu, M. Yu, Z. Huang and M. Fang, *Dalton Trans.*, 2019, **48**, 11791–11802.
27 M. Xia, X. Wu, Y. Zhong, H. T. Hintzen, Z. Zhou and J. Wang, *J. Mater. Chem. C*, 2019, **7**, 2927–2935.
28 I. L. Botto and M. Vassallo, *J. Mater. Sci. Lett.*, 1989, **8**, 1336–1337.
29 G. Blasse and B. C. Grabmaier, in *Luminescent Materials*, Springer Berlin Heidelberg, Berlin, Heidelberg, 1994, pp. 10–32.
30 G. Blasse, *J. Solid State Chem.*, 1986, **62**, 207–211.
31 G. Li, Y. Wang, W. Zeng, W. Chen, S. Han, H. Guo and Y. Li, *J. Mater. Chem. C*, 2016, **4**, 3304–3312.
32 L. G. Van Uitert, *J. Electrochem. Soc.*, 1967, **114**, 1048.
33 R. Naik, S. C. Prashantha, H. Nagabhushana, S. C. Sharma, B. M. Nagabhushana, H. P. Nagaswarupa and H. B. Premkumar, *Sens. Actuators, B*, 2014, **195**, 140–149.
34 Z. Li, B. Zhong, Y. Cao, S. Zhang, Y. Lv, Z. Mu, Z. Hu and Y. Hu, *J. Alloys Compd.*, 2019, **787**, 672–682.
35 Z. Yahiaoui, M. A. Hassairi, M. Dammak, E. Cavalli and F. Mezzadri, *J. Lumin.*, 2018, **194**, 96–101.
36 D. Geng, G. Li, M. Shang, C. Peng, Y. Zhang, Z. Cheng and J. Lin, *Dalton Trans.*, 2012, **41**, 3078.
37 L. Sun, B. Devakumar, J. Liang, S. Wang, Q. Sun and X. Huang, *J. Mater. Chem. C*, 2019, **7**, 10471–10480.
38 X. Hu, J. Fan, T. Li, D. Zhang, J. Bai, Z. Ren and X. Hou, *Chin. Sci. Bull.*, 2007, **52**, 444–449.
39 L. Zhiqi, R. Le, Z. Zhaowu, C. Dali, Z. Na, L. Minglai, C. Meisheng and H. Xiaowei, *J. Rare Earths*, 2006, **24**, 137–140.
40 D. L. Dexter, *J. Chem. Phys.*, 1953, **21**, 836–850.
41 G. Blasse, *J. Solid State Chem.*, 1986, **62**, 207–211.
42 X. Zhang, L. Zhou, Q. Pang, J. Shi and M. Gong, *J. Phys. Chem. C*, 2014, **118**, 7591–7598.
43 J. Sun, X. Zhang, Z. Xia and H. Du, *J. Electrochem. Soc.*, 2011, **158**, J368.
44 N. Guo, Y. Song, H. You, G. Jia, M. Yang, K. Liu, Y. Zheng, Y. Huang and H. Zhang, *Eur. J. Inorg. Chem.*, 2010, **2010**, 4636–4642.
45 Y. Chen, W. Ding, P. Li, X. Li, Q. Bao, J. Liu, K. Qiu, X. Meng, Z. Yang and Z. Wang, *RSC Adv.*, 2019, **9**, 30406–30418.
46 R. L. Tranquilin, L. X. Lovisa, C. R. R. Almeida, C. A. Paskocimas, M. S. Li, M. C. Oliveira, L. Gracia, J. Andres, E. Longo, F. V. Motta and M. R. D. Bomio, *J. Phys. Chem. C*, 2019, **123**, 18536–18550.
47 Y. Zhu, Y. Liang, M. Zhang, M. Tong, G. Li and S. Wang, *RSC Adv.*, 2015, **5**, 98350–98360.
48 P. A. Tanner, L. Zhou, C. Duan and K.-L. Wong, *Chem. Soc. Rev.*, 2018, **47**, 5234–5265.
49 J. Li, X. Zhou, J. Ding, X. Zhou and Y. Wang, *J. Mater. Chem. C*, 2019, **7**, 2257–2266.
50 B. Han, J. Zhang and Y. Lü, *J. Am. Ceram. Soc.*, 2013, **96**, 179–183.